KLOE memo n. 266/02

# Analysis of $\phi \to \eta'\gamma$ , $\phi \to \eta\gamma$ in $\pi^+\pi^-\gamma\gamma\gamma$ final state

F. Ambrosino
Università e Sezione INFN, Napoli

**Abstract**

A detailed description of the analysis of $\phi \to \eta\gamma$ , $\phi \to \eta'\gamma$ decays in $\pi^+\pi^-\gamma\gamma\gamma$ is presented. The ratio of the branching ratios of the two $\phi$ radiative decays has been measured to be $(4.70\pm0.47 \pm0.31)\cdot 10^{-3}$, leading to a very accurate determination of the mixing angle in the flavor basis $\varphi_P = (41.8^{+1.9}_{-1.6})^\circ$ and to the most accurate determination of BR($\phi \to \eta'\gamma$ ) to date: $(6.10 \pm 0.61 \pm 0.43) \cdot 10^{-5}$.

## 1 Introduction

Radiative decays of light vector mesons to pseudoscalars have been used as a useful testing ground since the early days of the quark model [1]. The branching ratio (BR) of the decay $\phi \to \eta'\gamma$ is particularly interesting since its value can probe the $|s\bar{s}\rangle$ and gluonium content of the $\eta'$[2]. In particular, the ratio of its value to the one of $\phi \to \eta\gamma$ can be related to the $\eta$-$\eta'$mixing parameters [3, 4, 5, 6, 7] and determine the mixing angle in the flavor basis $\varphi_P$ , which has been pointed out as the best suited parameter for a process-independent description of the mixing. In fact, within the two mixing-angles scenario which has emerged from an Extended Chiral Perturbation Theory framework [8], as well as from phenomenological analyses [9], has been demonstrated that the two mixing parameters in the flavor basis are equal apart from terms which violate the Okubo-Zweig-Iizuka (OZI) rule [10, 11], and is thus safe to use one single mixing angle in this basis. The measurements available to date on BR($\phi \to \eta'\gamma$ ) have still rather large statistical uncertainties [12, 13]. The present analysis of $\phi \to \eta'\gamma$ decays is based on an integrated luminosity of $\simeq 16\,\mathrm{pb}^{-1}$ corresponding to about 60% of the luminosity collected by the KLOE detector [14] at the DA$\Phi$NE [15] $e^+e^-$ collider in Frascati during year 2000. The accuracy we obtain is significantly better than the current world average and allows us to extract the $\eta$-$\eta'$mixing angle in the flavor basis with an error of $\simeq 1.5^\circ$ from this single measurement.

## 2 Final state choice

We use the following decay chains to determine the ratio $R = BR(\phi \to \eta'\gamma)/BR(\phi \to \eta\gamma)$:

* $\phi \to \eta'\gamma$ ;
  - $\eta' \to \pi^+\pi^-\eta$;
    - $\eta \to \gamma\gamma$

* $\phi \to \eta\gamma$ ;

  $\eta \to \pi^+\pi^-\pi^0$ ;

  $\pi^0 \to \gamma\gamma$

The final state is $\pi^+\pi^-\gamma\gamma\gamma$ for both the $\phi \to \eta'\gamma$ and $\phi \to \eta\gamma$ events, and thus most of the systematics approximately cancel out when evaluating the ratio $R$; moreover since the $\phi \to \eta\gamma$ decays can be quite easily selected with small background they constitute a very clean control sample for the analysis. We will see in more detail this in the next sections. The $\phi \to \eta\gamma$ events, being about two orders of magnitude more abundant than the corresponding $\phi \to \eta'\gamma$ ones, constitute also the main source of background for the $\phi \to \eta'\gamma$ detection. Further background events can rise from:

* $\phi \to K_S\, K_L$ events with one charged vertex where at least one photon is lost and the $K_L$ is decaying near the interaction point (IP);
* $\phi \to \pi^+\pi^-\pi^0$ events with an additional photon detected due to accidental photons or splitting of clusters in the electromagnetic calorimeter (EmC).

# 3 Selection: first level

The events are reconstructed using the standard KLOE reconstruction libraries. For this analysis the events were reconstructed using DATAREC version 7. They were selected by the charged radiative filter PPFILT [16] which manages to reduce background from $\phi \to K_S\, K_L$ , machine background, Bhabha and cosmic rays events. After this selection a very loose topological selection is applied in order to reduce the number of events in input to the kinematic fit, dropping the huge amount of Bhabha (and radiative Bhabha) events which are still present in the RAD stream.

Events surviving this selection have been written on disk in (compressed) YBOS format and fed in input to the kinematic fit procedure.

Let us analyze the various steps in some detail.

## 3.1 Trigger

Due to the presence of high energy photons in both categories of events, the trigger efficiency is very high for these samples. The two efficiencies are found to be 98.6% and 98.9% respectively for $\phi \to \eta\gamma$ and $\phi \to \eta'\gamma$ events, the ratio being very close to 1. The matching between the trigger sector multiplicities from Monte Carlo and the ones for real data has been checked for the $\phi \to \eta\gamma$ control sample, and is shown in fig. 1. The agreement between the selected $\phi \to \eta\gamma$ data set and the Monte Carlo distributions is good. Moreover the overall inefficiency induced by trigger on the analysis is very small due to correlation with EVCL and topological selection efficiencies. In fact the trigger efficiency on the sample of events which pass both the EVCL and topological selections goes to 99.9% for both categories of events. We will thus use trigger efficiency evaluated by Monte Carlo neglecting any systematic bias introduced by the trigger in what follows.

## 3.2 FILFO

The machine background filter (FILFO) procedure has a good efficiency for both samples for the triggered events (94.6% for $\phi \to \eta\gamma$ and 96.1% for $\phi \to \eta'\gamma$ ) . Since DATAREC version 7 has been used for the

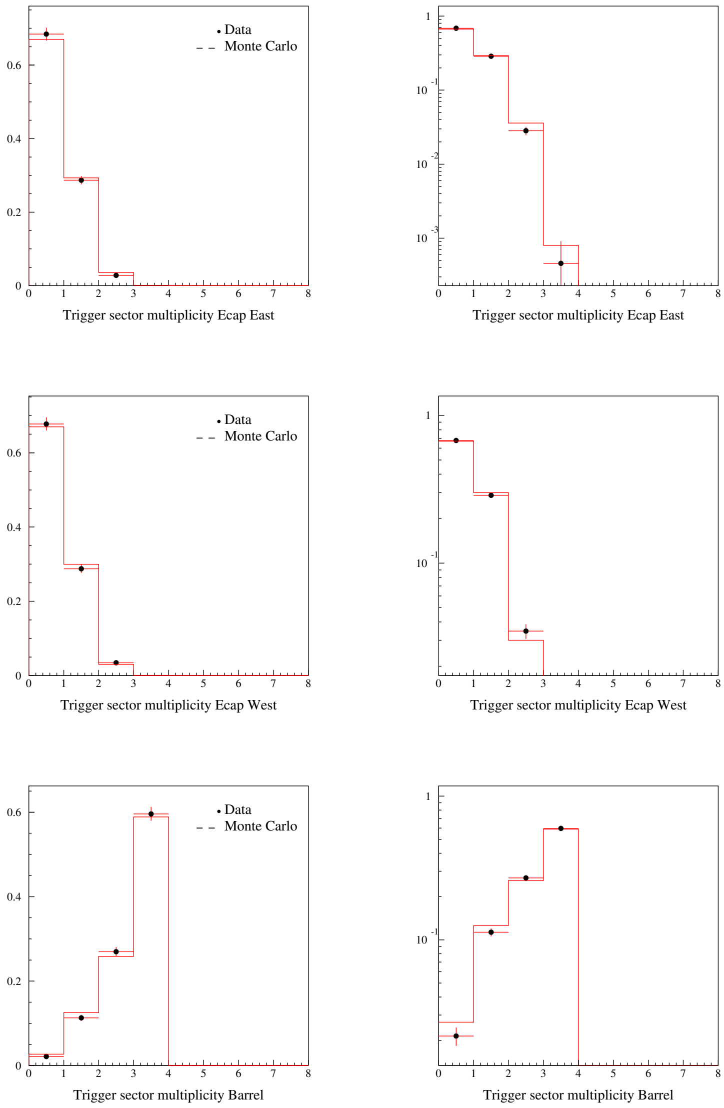


Figure 1: Trigger sector multiplicity. From top to bottom: endcap East, endcap West, barrel. Plots on the right are the same but in log scale.

analysis, the inefficiency introduced by FILFO for the radiative events is small, and the selection is much more stable than it was in the past. It was in fact recognized, on previous versions of the reconstruction, that the Bhabha filter in FILFO was rejecting radiative events depending on the number of hits in the drift chamber, and hence on the machine background conditions. In order to solve this problem the neutral radiative filter used in the Event Classification procedure has been applied also to the events at FILFO level (where no tracks are reconstructed yet). Events passing this filter ($\phi$ radiative decays in both fully neutral and charged/neutral final state) are not rejected by FILFO. Since the Event Classification procedure [16] essentially selects prompt clusters, the overall efficiency $\varepsilon_{FILFO \cdot EVCL}$ is expected to be pretty much the same as $\varepsilon_{EVCL}$, and it is really indeed what Monte Carlo evaluations show (see table 1).

| Events | $\varepsilon_{FILFO}$ | $\varepsilon_{EVCL}$ | $\varepsilon_{FILFO \cdot EVCL}$ |
|---|---|---|---|
| $\phi \to \eta\gamma$ | 94.6% | 59.6% | 59.3% |
| $\phi \to \eta'\gamma$ | 96.1% | 55.8% | 55.6% |

Table 1: Monte Carlo efficiency on triggered events: only FILFO (first column), only EVCL (second column) and both selections (last column). The strong correlation is evident.

### 3.3 Cosmic veto

The cosmic veto acts both at the trigger level, and at software level. The overall scale factor for events triggering the cosmic veto is 50. The probability for a pion to fire a cosmic veto sector has been evaluated directly on data as a function of the pion momentum within the $\pi\pi\gamma$ analysis [17]. The strategy followed is to evaluate how many times one pion fires the cosmic veto when the other one does not, and then correct for the correlation. As expected, this probability is strongly momentum dependent, and is almost negligible for pion total momentum below 200 MeV/c. It has been evaluated in slices 5° wide in $\theta$. A typical shape for one $\theta$ slice, separately for $\pi^+$and $\pi^-$is shown in fig. 2. We have used this distributions, together with "true" Monte Carlo information for pions momenta and angles to evaluate the *a priori* inefficiency induced by the cosmic veto for both $\phi \to \eta\gamma$ and $\phi \to \eta'\gamma$ events. The number obtained is $\mathcal{O}(10^{-5})$ for $\phi \to \eta\gamma$ and even less of $\phi \to \eta'\gamma$ before any other cut. Thus the effect of cosmic veto has been neglected in what follows.

### 3.4 Event Classification

The cuts used in the event classification procedure to select radiative events with charged particles are the following [16]:

- Charged vertex in region $\rho < 8$ cm, $|z| < 15$ cm
- Cut in plane $\delta E_\gamma$ vs $P_{\pi^+} + P_{\pi^-}$ (see fig. 7)
- Total energy of prompt unassociated clusters between 350 and 800 MeV.
- $n_\gamma > 3$ or ($1 < n_\gamma < 4$ and hardest photon energy $> 250$ MeV)

(where $n_\gamma$ stands for the number of prompt neutral clusters).

The variable $\delta E_\gamma$ is defined as follows:

$$\delta E_\gamma = |\overrightarrow{p_1} + \overrightarrow{p_2}| - \left(M_\phi - \sqrt{m_\pi^2 + |\overrightarrow{p_1}|^2} - \sqrt{m_\pi^2 + |\overrightarrow{p_2}|^2}\right)$$

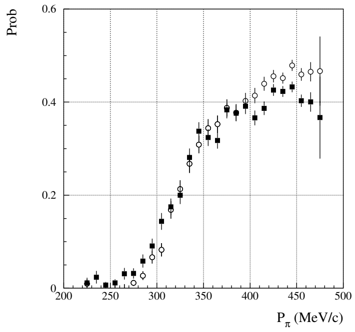


Figure 2: Probability to fire a cosmic veto sector as a function of the pion momenta. The curve refers to a slice $35° \leq \theta \leq 40°$ and is shown separately for $\pi^+$(dots) and $\pi^-$(squares).

It has the properties to be exactly zero for $\pi\pi$ and $\pi\pi\gamma$ final states, and always negative for final states with two charged pions and more than two photons. The EVCL efficiency is largely dominated by the charged vertex reconstruction efficiency. In table 2 we show, apart from any other effect (trigger, FILFO and so on) the charged vertex reconstruction efficiency and the overall EVCL efficiency as evaluated by Monte Carlo for both categories under study. It is remarkable to see that the bulk of the difference in

| Events | $\varepsilon_{VTX}$ | $\varepsilon_{EVCL}$ |
|---|---|---|
| $\phi \to \eta\gamma$ | 62.7% | 59.6% |
| $\phi \to \eta'\gamma$ | 59.0% | 55.8% |

Table 2: Monte Carlo efficiency: charged vertex (first column), and EVCL (second column)

EVCL efficiency between the two samples is due to the difference in charged vertex efficiency, while the other EVCL cuts have $\simeq 95\%$ efficiency for both categories of events where a $\pi^+\pi^-$ vertex is found.

Since reconstruction efficiency depends essentially on momentum distributions of the tracks we have checked by Monte Carlo tracking efficiency as function of momenta for the two samples as well as vertex efficiency as a function of the minimum pion momentum. The results are shown in figs. 3,4. As expected the momentum dependence of the efficiencies are very similar for the two samples, and the main difference is in the momentum distribution of the pions in $\phi \to \eta'\gamma$ events with respect to $\phi \to \eta\gamma$ ones.

A good check of the Monte Carlo performance in evaluating the efficiency comes from the distributions of $P_T$, $P_z$ and $\cos\theta$ of the pions in the $\phi \to \eta\gamma$ control sample on data. Comparing the distributions with the ones expected by Monte Carlo one can check if a significant bias in some momentum region is present on data: a Monte Carlo - data discrepancy in some region of the spectrum should in principle show up in this way. The results of this check are shown in fig. 5. The agreement is very good on all the spectra, and is evident in both linear and logarithmic scale plots. Some very small background (O(0.3%)) is still present on $\phi \to \eta\gamma$ selected events.

The absence of a bias in the distributions tells us only that the profile of the dependence of efficiency on pion momenta is well reproduced by Monte Carlo, not providing any check of the absolute value of the efficiency itself. However, if for some reason (e.g. presence of spurious hits in the chamber which let the track fit become unstable) the absolute efficiency on data is lower by just a scale factor with respect to

Monte Carlo one, this effect will cancel out in the ratio between the two channels. As a further check the whole analysis has been repeated selecting $\phi \to \eta\gamma$ events only in the kinematic region of $P_T < 200 MeV$ allowed to $\phi \to \eta'\gamma$ pions. Results are summarized later on, in table 5.

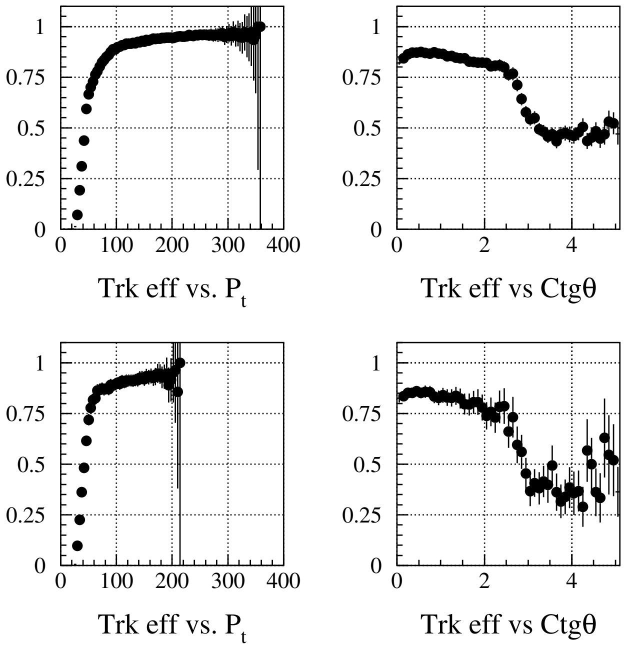


Figure 3: Tracking efficiency versus $P_T$ and $\cot\theta$ for $\phi \to \eta\gamma$ (upper plots) and $\phi \to \eta'\gamma$ events.

The cuts on the vertex position in EVCL are loose enough to give no significant acceptance problem. In our topological selection we use somewhat tighter cuts, in order to help reducing the $\phi \to K_S\, K_L$ background. Again, comparison between data and Monte Carlo for the control sample is very satisfactory (see fig. 6). The effect of the shift of about 9 mm in the z coordinate of the vertex position (due to the DAΦNE beam crossing position during these runs) has been evaluated on Monte Carlo to be totally negligible ($\Delta\varepsilon = 0.01\%$). Apart from this shift the distributions show a different width, as the results of the Gaussian fit clearly show. This is due to a beam length in z , as simulated in Monte Carlo, larger with respect to the real one. The analysis cuts however are loose enough to let this effect (which moreover is common to both categories) be negligible.

The distribution for the variables relevant to the remaining EVCL cuts on the $\phi \to \eta\gamma$ control sample are shown in figs. 7,8. Agreement with expected distributions is again very good.

The checks performed above show that the variables on which the EVCL cuts are set are well reproduced in the Monte Carlo simulation and allow us to trust the Monte Carlo based EVCL efficiencies.

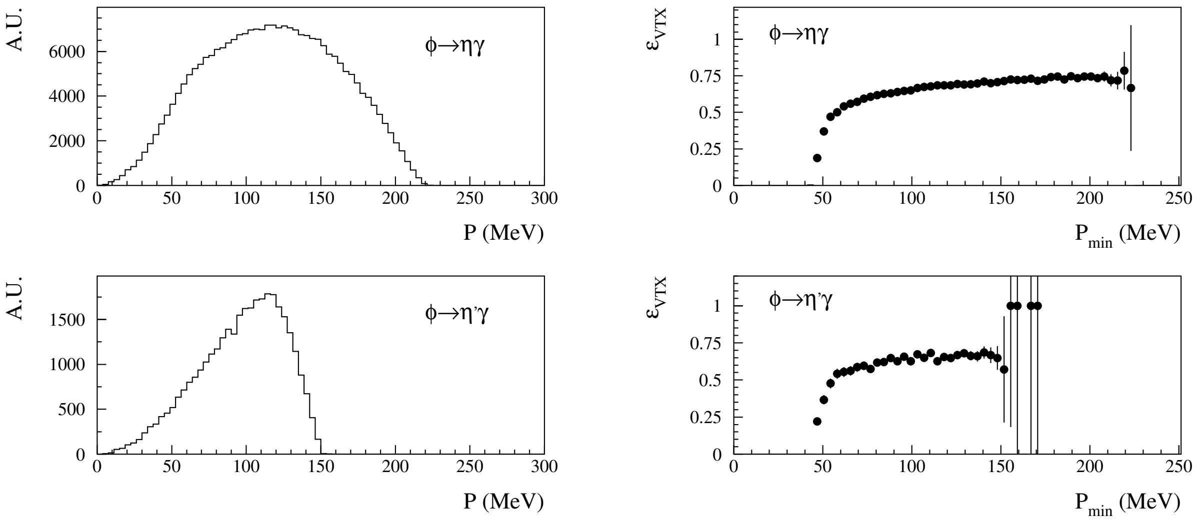


Figure 4: Left: Minimum momentum among the two pions for $\phi \to \eta\gamma$ and $\phi \to \eta'\gamma$ . Right: Vertex efficiency versus the minimum momentum.

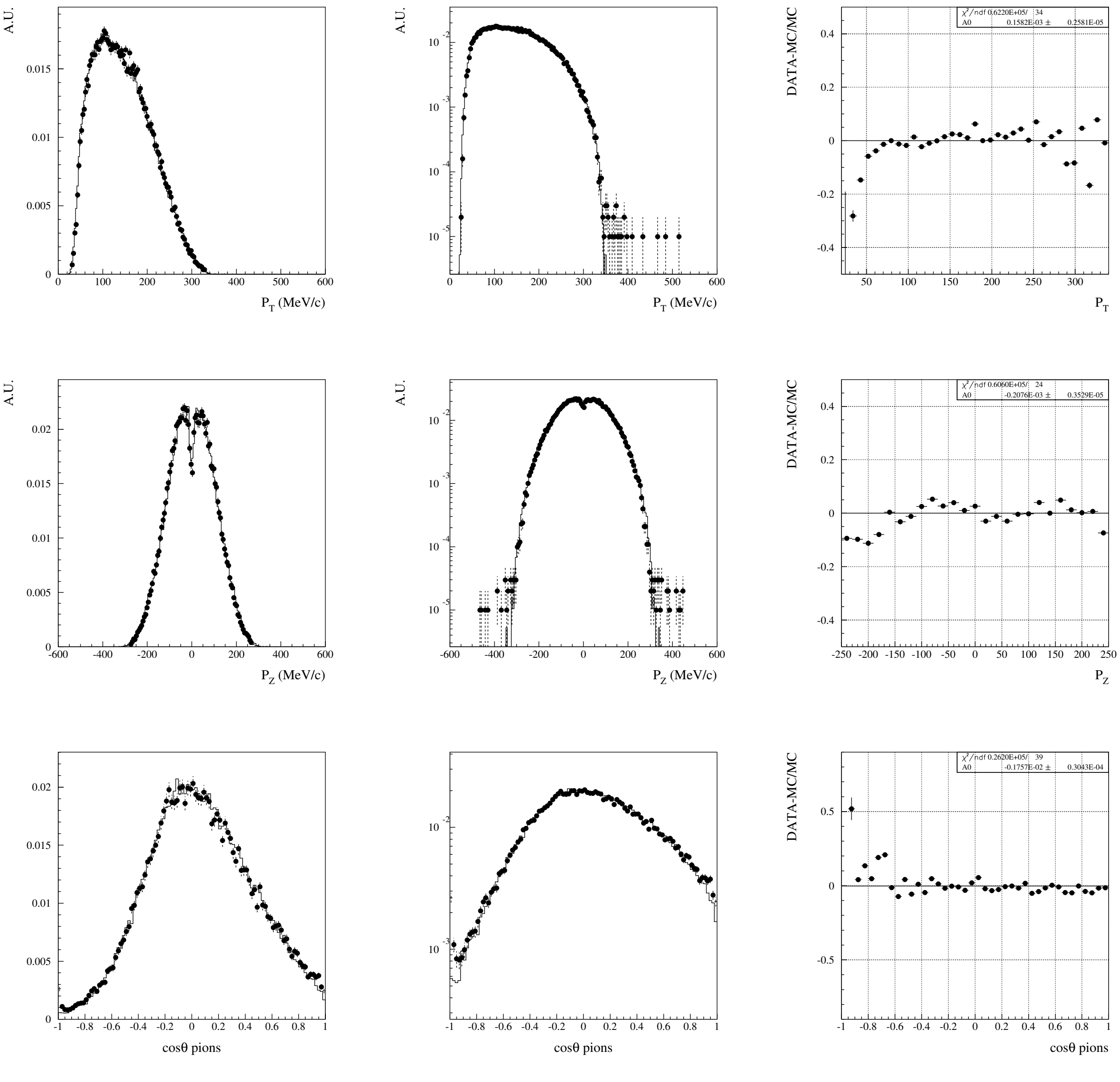


Figure 5: Data vs Monte Carlo comparisons $\phi \to \eta\gamma$ events. From top to bottom: $P_T$, $P_Z$, $\cos\theta$ between pion tracks. Left: linear scale. Center: log scale. Right: Bin by bin normalized DATA-MC discrepancy.

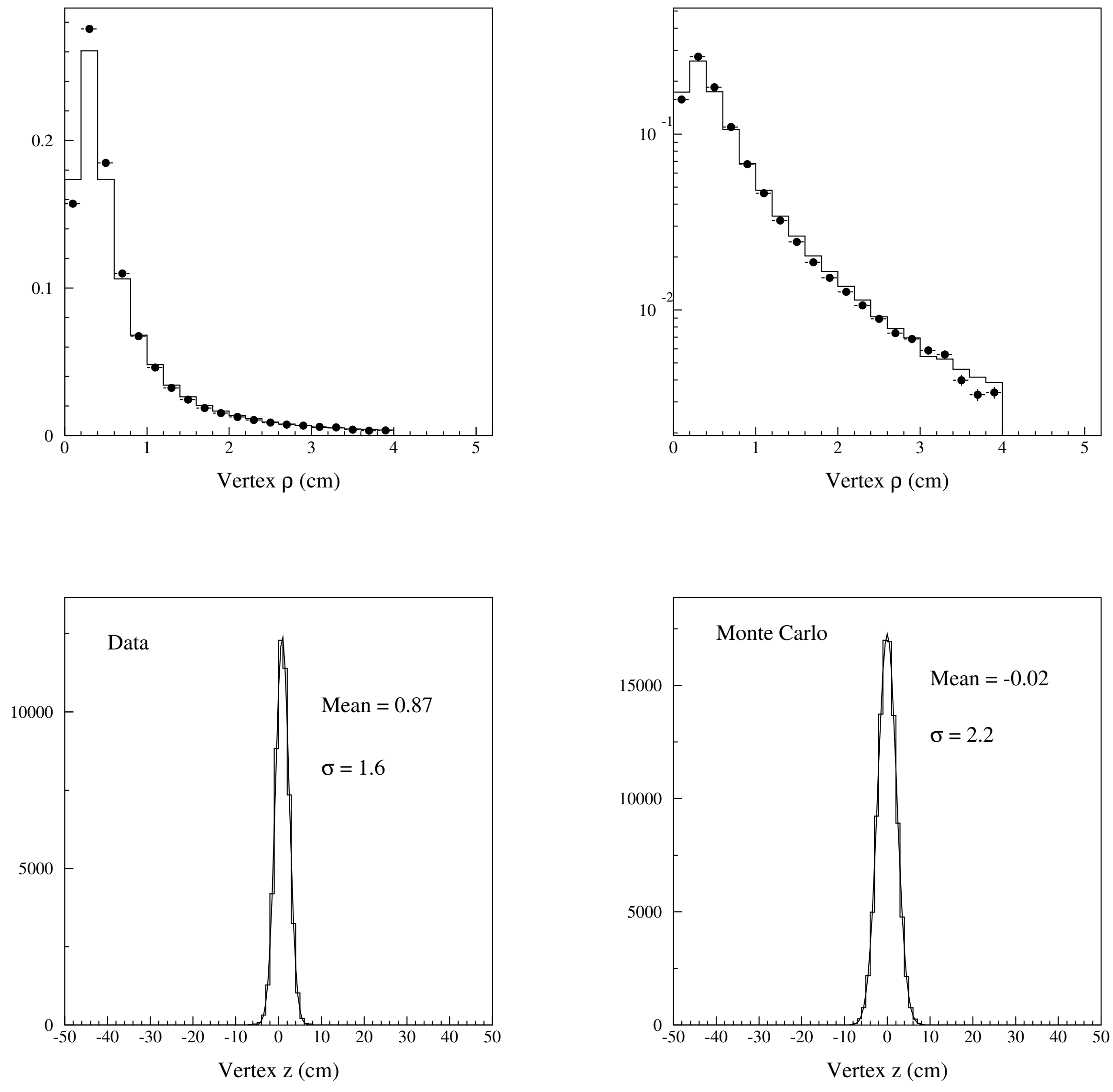


Figure 6: From top left in clockwise direction: data MC comparison on charged vertex position in xy plane in linear scale; same but in log scale; vertex z position on Monte Carlo; same on $\phi \to \eta\gamma$ selected data.

As a further, independent check of the systematic bias introduced by EVCL we have analyzed the same sample of data *without any EVCL selection.* The raw data selected only by FILFO have been first preselected using a very simple topological selection:

- number of prompt clusters above $18° > 2$

- Total energy in Emc $> 600$ MeV

and then reconstructed and analyzed with the standard analysis described in the following sections. The results of this study have been summarized in section 4.4.

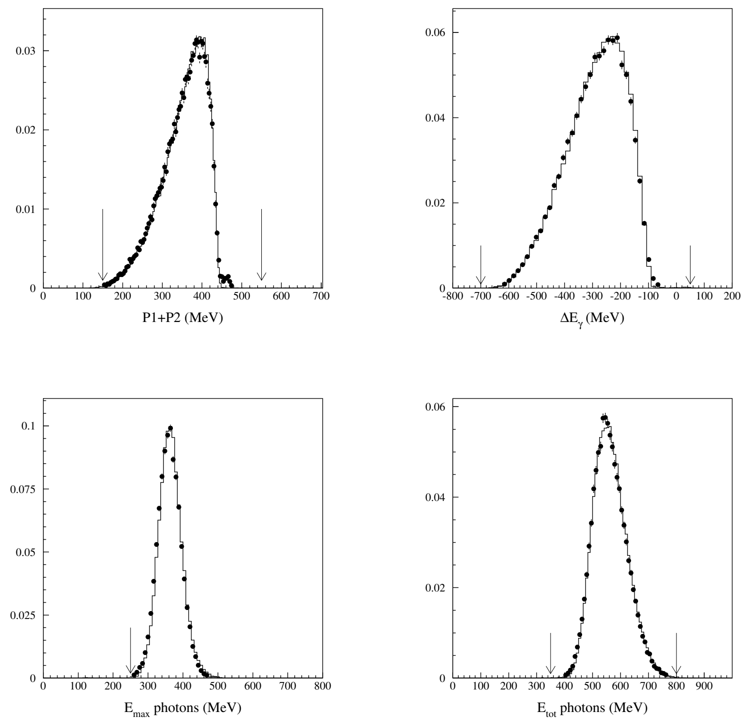


Figure 7: Variables used in EVCL: the arrows show the position of the selection cuts.

## 3.5 Topological cuts

Before performing the kinematic fit a simple topological selection is done. We ask, thus:

- 3 and only 3 prompt neutral clusters (see below) with $21° < \theta_\gamma < 159°$ and $E_\gamma > 10$ MeV

- Opening angle between each couple of photons $> 18°$

- 1 charged vertex inside the cylindrical region $r < 4$ cm; $|z| < 8$ cm.

A prompt neutral cluster is defined as a cluster in the EmC with no associated track coming from the Drift Chamber (DC) and $|(t - \frac{r}{c})| < 5\sigma_t$ where $t$ is the arrival time on the EmC, $r$ is the distance of the cluster from the IP and $c$ is the speed of light and $\sigma_t = 54\,\mathrm{ps}/\sqrt{E(\,\mathrm{GeV})} \oplus 147\,\mathrm{ps}$[19].

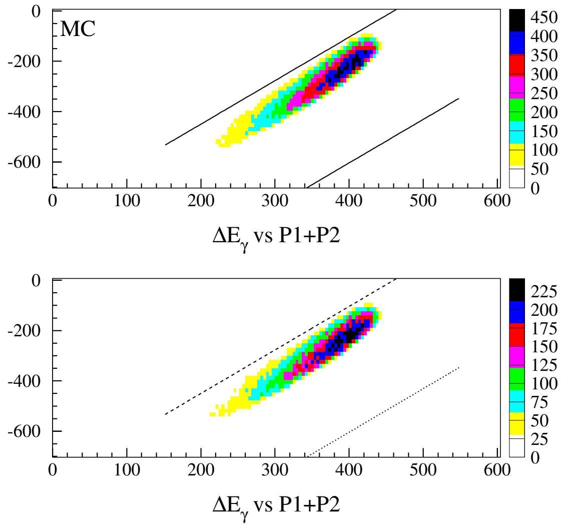


Figure 8: Scatter plot of $\delta E_\gamma$ vs. $|P_1| + |P_2|$ for MC (upper plot) and DATA (lower plot). The lines show the selection region.

The cut at 10 MeV minimum energy strongly reduces the *inefficiency* induced by a wrong cluster counting when small cluster fragments are reconstructed as a different cluster (cluster splitting). Moreover it helps scaling down soft machine background photons.

The region below 21° is excluded due to the presence of DAΦNE magnetic quadrupoles near the interaction point.

The cut on the opening angle of the photons again reduces the problem of cluster splitting. In fact the splitting affects clusters which have a small angular separation ($< 15°$).

### 3.6 Systematic checks

The overall "common" selection efficiencies (including trigger, reconstruction, event classification and first level topological selection) are 39.33% and 43.58% respectively for $\phi \to \eta'\gamma$ and $\phi \to \eta\gamma$ events.

The ratio of the two efficiencies $\varepsilon_{\eta'\gamma}/\varepsilon_{\eta\gamma} = 0.902$ is reasonably close to one, as expected. As already noticed the main reason for this ratio not being one is the difference in the efficiency to find a charged vertex; this in turn is related to a different momentum spectrum of charged pions in the two categories of events.

This ratio has been used in extracting the value of $\Gamma(\phi \to \eta'\gamma\ )/\Gamma(\phi \to \eta\gamma\ )$ from the number of observed events in the two channels. As already noticed, given the matching between data and simulated distribution for almost all variables considered, no systematic correction at first level has been applied with respect to the Monte Carlo value.

In order to give an estimate of the possible systematic error introduced using this number we have checked its stability with respect to several independent shifts/distortions of the physical variables involved or displacement of the cuts, in some cases (such as for the clusters times) in a somewhat conservative way. The results we obtained have been summarized in table 3.

The effects of accidental clusters in time window on the photon counting efficiency is, by definition, independent on the channel under study if we choose the same time window definition for the two categories of events, and thus cancels out in the ratio. This has been confirmed by a Monte Carlo study in which the accidental cluster simulation tuned on the year 2000 run conditions is added by means of the ACCELE module [20]. Results are shown in the last line of table 3 .

The effect of cluster splitting is seen fully as an inefficiency for both channels. In fact the angular separation cut ensures that is very unlikely that one photon lost by acceptance is "substituted" in the counting by a split photon. Thus the net effect of splitting is to have some percentage of events in which four (or more) photons are counted instead of three, being in this way rejected by the topological selection algorithm.

A study performed on $\phi \to \eta\gamma \ \to 7\gamma$ sample has shown that the single cluster splitting probability on data is approximatively twice as the one evaluated by Monte Carlo [21].

Even if this effect can be significant (at level of some %) for the single channel efficiencies evaluated via Monte Carlo, it is again expected to cancel out, at least at first order, in the ratio of the two.

To evaluate the effect on the ratio we proceeded in this way:

- Evaluate the effect of photon splitting inefficiency by Monte Carlo on both channels via the ratio

$$\frac{N_{>3}}{N_3 + N_{>3}}$$

  where the suffix indicates the number of prompt neutral clusters above 21°.

- Suppose the *difference* among inefficiencies between the two channels is doubled on data, and goes straight into the final real selection efficiencies.

- Evaluate the shift on the ratio of efficiencies caused by this discrepancy.

The splitting inefficiencies as described above have been evaluated to be 2.62% and 2.48% respectively for $\phi \to \eta\gamma$ and $\phi \to \eta'\gamma$ events. The difference among splitting inefficiencies is 0.14%. Doubling this value to 0.3% we get a new efficiency ratio which is moved by +0.006 w.r.t. the central Monte Carlo value.

We decide to add in quadrature all the contributions in table 3 with this final (largest) contribution to get an estimate of 0.8% systematic uncertainty on the ratio of first level efficiencies.

| Effect | $\Delta\varepsilon_{\eta\gamma}$ | $\Delta\varepsilon_{\eta'\gamma}$ | $\Delta\left(\frac{\varepsilon_{\eta'\gamma}}{\varepsilon_{\eta\gamma}}\right)$ |
|---|---|---|---|
| $\Delta$E = ±2% | ±0.1% | ±0.1% | ±0.001 |
| $\Delta$t = ±200 ps | −2.4% | −2.1% | +0.002 |
| $\Delta\theta_\gamma = +1°$ | −0.9% | −0.7% | +0.003 |
| Accidental clusters added | −0.1% | −0.1% | −0.001 |

Table 3: Stability of the common analysis efficiency ratio.

# 4 Selection: second level

## 4.1 Kinematic fit

After the first level selection we perform a kinematic fit constraining global energy-momentum conservation and the speed of light for each photon, without imposing any intermediate particle mass constraint.

The inputs to the fit are:

- E, x, y, z, t for each photon
- x, y, z position of the vertex
- $P_T$, $\cot\theta$ and $\phi$ at vertex for each track
- Beam energies

for a total of 26 parameters. The number of constraints (7) is also the number of degrees of freedom of the fit, as usual in a kinematic fit.

The kinematic fit is performed using a standard Lagrange multipliers technique. The effect of this fit on the event reconstruction is to improve significantly (by factors two to four) the resolution on photon energies and invariant masses.

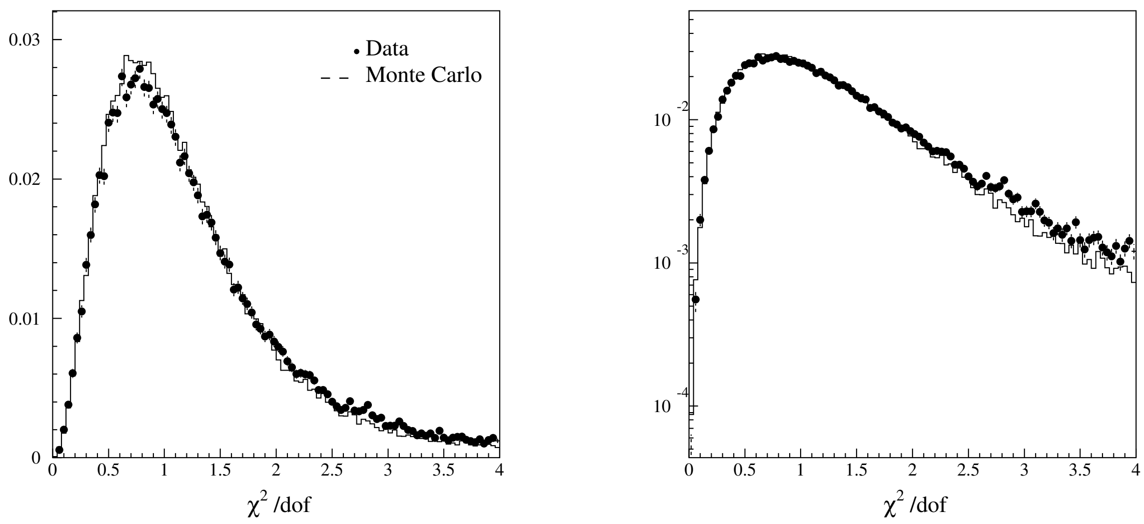


Figure 9: $\chi^2$ per degree of freedom distribution on $\phi \to \eta\gamma$ events. Left: linear scale; Right: log scale.

A loose cut on $\mathcal{P}(\chi^2) > 1\%$ for this fit is imposed for both $\phi \to \eta\gamma$ and $\phi \to \eta'\gamma$ events to ensure the good reconstruction of the event. After a first analysis using the "nominal" Monte Carlo values for the various parameters entering the fit the distribution of the $\chi^2$ variable showed a slightly different behavior on data and Monte Carlo for the $\phi \to \eta\gamma$ sample.

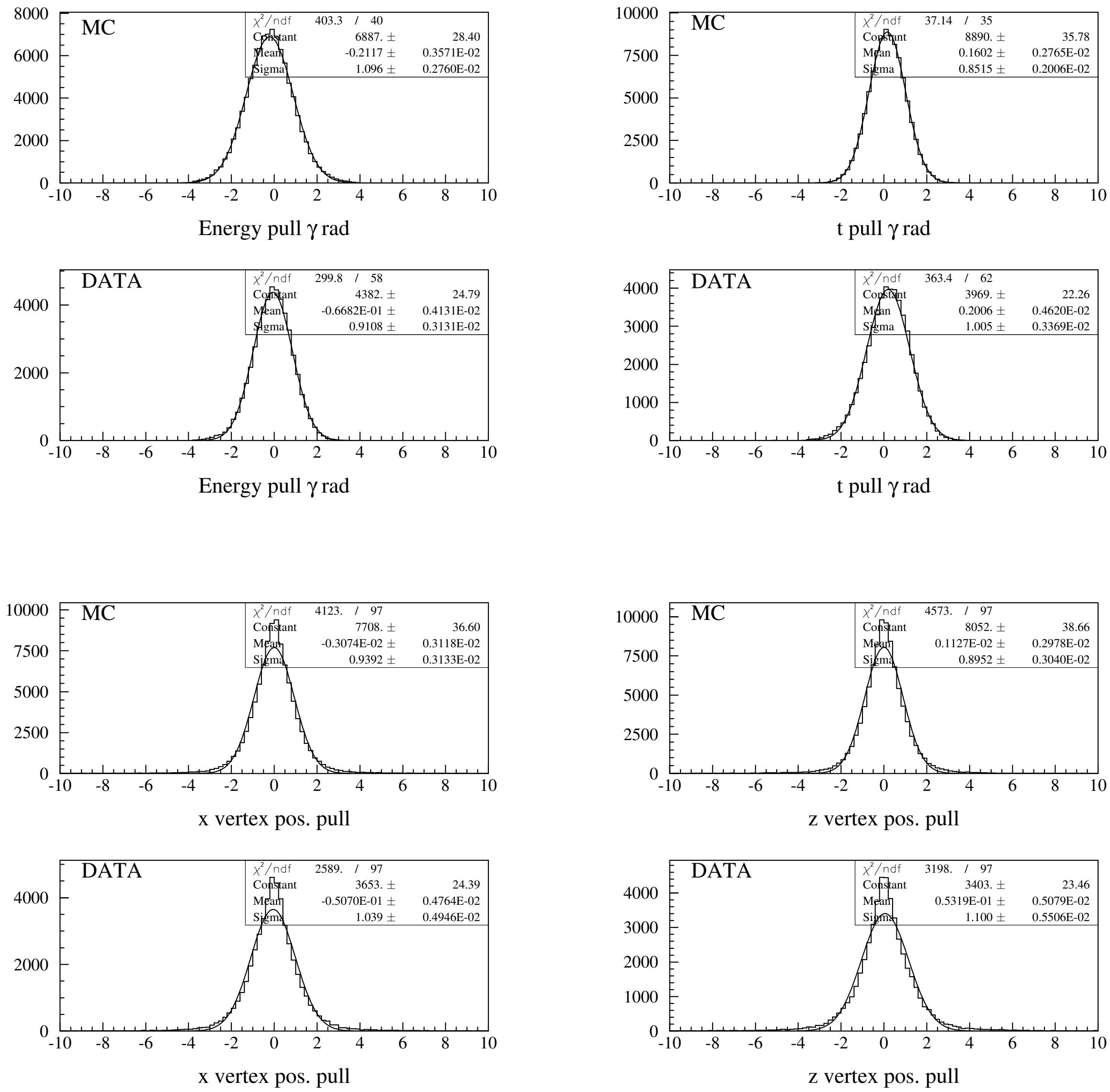


Figure 10: Data MC comparison for various fit pulls before the renormalization of errors on Monte Carlo.

A study of the pulls[1] of the fit has shown that this worsening of the chisquare is not due to a single input parameter of the fit: indeed all distributions show a very reasonable behavior but some of them (such as cluster times and vertex positions) slightly ($\approx 10 - 15\%$) broader than the expected. We have thus "renormalized" the Monte Carlo values for the resolution on these parameters (namely positions and times of the clusters) using the ratio of the pulls between data and Monte Carlo. In this way, as expected, a good agreement of the $\chi^2$ variable is observed (see fig. 9). We believe that this procedure is correct since:

- No single effect was dominating the $\chi^2$ value signalling thus a sizeable reconstruction problem;
- No crucial background subtraction is performed cutting on $\chi^2$ probability in the final selection. We just use kinematic fit as a mean to improve reconstruction and use a loose cut on $\mathcal{P}(\chi^2)$ to ensure kinematic closure of the events.
- The distributions of the initial values for the total four momentum show a very reasonable behaviour for the $\phi \to \eta\gamma$ control sample.

## 4.2 $\phi \to \eta\gamma$ events selection

Apart from the first level selection, the only additional cuts to select $\phi \to \eta\gamma$ events are a $\pm 10\ \sigma$ cut on the energy of the radiative photon (after kinematic fit) and a cut on pion energy endpoint. We require thus:

* $320\,\mathrm{MeV} < E_\gamma^{\mathrm{rad.}} < 400\,\mathrm{MeV}$
* $E_{\pi^+} + E_{\pi^-} < 550\,\mathrm{MeV}$

The first cut has almost 100% efficiency on the signal and is very effective in reducing residual background from $\phi \to K_S\,K_L$ events where the endpoint for photon energies is at 280 MeV. The second cut is also fully efficient on signal and eliminates residual $\phi \to \pi^+\pi^-\pi^0$background. After this cuts we are left with $N_{\eta\gamma} = (502.1 \pm 2.2) \cdot 10^2$ events, and the overall efficiency in detecting $\phi \to \eta\gamma$ events is evaluated from Monte Carlo to be 36.5%. Expected background is below 0.5%, and all the distributions observed are in agreement with this estimate. The abundant and pure $\phi \to \eta\gamma$ events can be used as control sample to evaluate systematic effects on the efficiency by comparing data versus Monte Carlo distributions for the variable on which the cuts are set.

## 4.3 $\phi \to \eta'\gamma$ events selection

Background from $\phi \to \pi^+\pi^-\pi^0$ events is strongly reduced by means of a cut on the charged pions energy endpoint:

* $E_{\pi^+} + E_{\pi^-} < 430\,\mathrm{MeV}$ ($\phi \to \eta'\gamma$ events)

Further selection of $\phi \to \eta'\gamma$ events is made via a cut on the total photon energy (to scale down $\phi \to K_S\,K_L$ background):

[1] We recall that for a measured parameter $P_{meas}$ which is fitted to the value $P_{fit}$ the pull is defined as $\frac{P_{meas} - P_{fit}}{\sqrt{\sigma^2_{meas} - \sigma^2_{fit}}}$ and is expected to be distributed as the normal Gaussian distribution N(0,1).

* $\Sigma_\gamma E_\gamma > 540\,\mathrm{MeV}$.

Contamination from $\phi \to \eta\gamma$ events into the $\phi \to \eta'\gamma$ sample is at this level still very high since about 35% of $\phi \to \eta\gamma$ events are still in the sample (S/B $\approx 5 \cdot 10^{-3}$) while contamination from $\phi \to K_S\,K_L$ and $\phi \to \pi^+\pi^-\pi^0$ is expected to be small. In fact no Monte Carlo generated event from $\phi \to K_S\,K_L$ and $\phi \to \pi^+\pi^-\pi^0$ survives these cuts giving rise to upper limits on these backgrounds (dominated, in the present analysis, by limited Monte Carlo statistics) given by, respectively:

* $N_{K_S\,K_L} < 2.5 \cdot 10^{-7} \cdot N_\phi$ at 90% C.L.

* $N_{\pi^+\pi^-\pi^0} < 1 \cdot 10^{-7} \cdot N_\phi$ at 90% C.L.

This would result in $N_{bkg} < 18$ events @ 90% C.L. *before any further cut.*

To select $\phi \to \eta'\gamma$ events over the $\phi \to \eta\gamma$ background we exploit the kinematical properties of the three photon in both categories of events. The energy spectrum of the photons gives no combinatorial problem : radiative photon is the hardest one in $\phi \to \eta\gamma$ events, while it is the softest in $\phi \to \eta'\gamma$ events; the other two photons being generated in $\pi^0$ and $\eta$ decays respectively (fig. 11). If we plot the energy

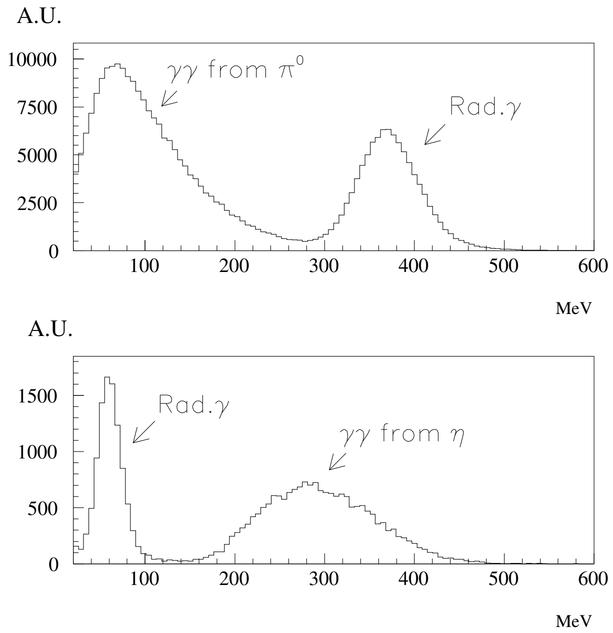


Figure 11: Monte Carlo photon energy spectrum for $\phi \to \eta\gamma \to \pi^+\pi^-\gamma\,\gamma\,\gamma$ (upper plot) and $\phi \to \eta'\gamma \to \pi^+\pi^-\gamma\,\gamma\,\gamma$ (lower plot).

of the two hardest photons (chosen at random to be "$E_1$" and "$E_2$") after kinematic fit we see (fig. 12) that a strong correlation between the two photons from $\eta$ is present in $\phi \to \eta'\gamma$ events while the $\phi \to \eta\gamma$ events are grouped into two bands around $E_{1(2)} = 363$ MeV as expected from the presence of the nearly monochromatic radiative photon. The selection of $\phi \to \eta'\gamma$ events is then made cutting on an elliptic shaped region in the $E_1 - E_2$ plane whose parameters are:

* Coordinates of the ellipse center = (285,285) MeV

* Major axis = 90 MeV

* Minor axis = 25 MeV
* Major axis inclination w.r.t. $E_1$ axis = 135°

The value of the minor axis and of the center of the ellipse have been chosen according to the MC distribution (see again fig. 12). Then, the value of the major axis cut has been varied in the range between 25 and 100 MeV and the quantity $N_S/\sqrt{N_B}$ has been evaluated for each value considered. The value chosen is the one maximizing this quantity.

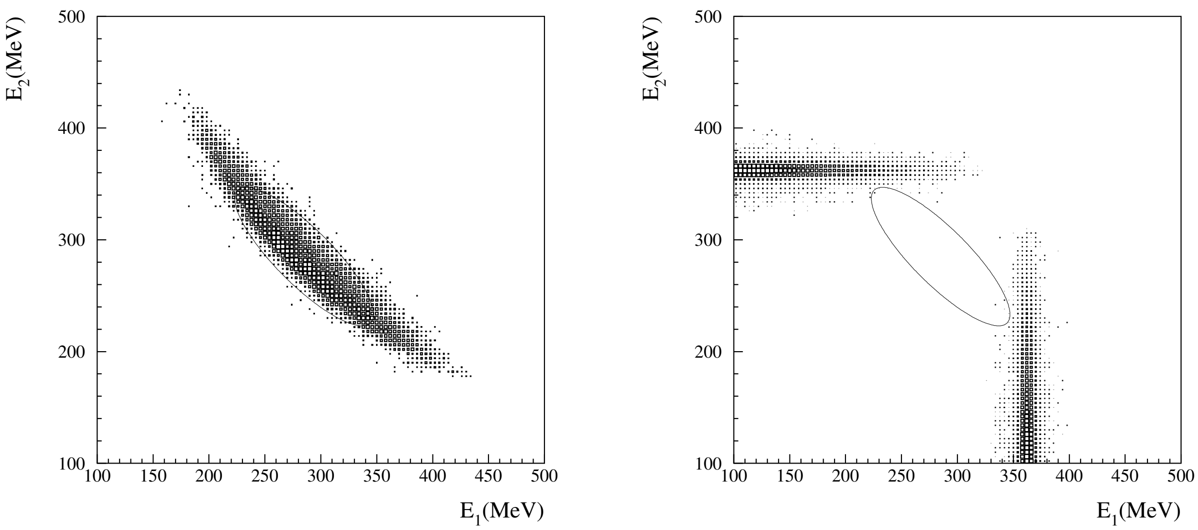


Figure 12: Left: Monte Carlo $\phi \to \eta'\gamma$ events in the $E_1 - E_2$ plane; Right: Monte Carlo $\phi \to \eta\gamma$ events in the $E_1 - E_2$ plane. The elliptical selection region is shown.

If we plot the $\pi^+\pi^-\gamma\gamma$ invariant mass for the events inside the selection ellipse on data we notice a clear peak at the $\eta'$ mass value with the same $\sigma$ of the one expected from Monte Carlo, over a small residual background (see fig.15). The signal has been thus selected in the region $942\,\mathrm{MeV}/c^2 \leq M_{\pi^+\pi^-\gamma\gamma} \leq 974\,\mathrm{MeV}/c^2$ and the evaluated background subtracted.

#### 4.3.1 Backgrounds

The distribution of the two hardest photons energies on the selected data sample is shown in fig 13. In addition to the foreseen $\eta$ bands at about 360 MeV and to the $\eta'$band in the selection region, some more events are present in the plot. These events are not foreseen within our Monte Carlo generated backgrounds, and have to be somehow investigated. For this reason we select events inside a *control region* which is an ellipse with the same area as the signal selection one but with the center shifted at 240 MeV, where no signal is expected. If we plot the $\pi^+\pi^-\gamma\gamma$ invariant mass for these event we clearly see that it is peaked to lower values w.r.t. the expected $\phi \to \eta'\gamma$ signal (see fig. 14). Moreover if we plot the $\gamma\gamma$ invariant mass for each possible coupling of two out of the three photons, we clearly see a nice peak at the $\pi^0$ value, signalling that these events are not signal events. These events can however be responsible for the higher background observed on the left of the $\eta'$mass peak w.r.t. the one foreseen by only considering $\phi \to \eta\gamma$ background events.

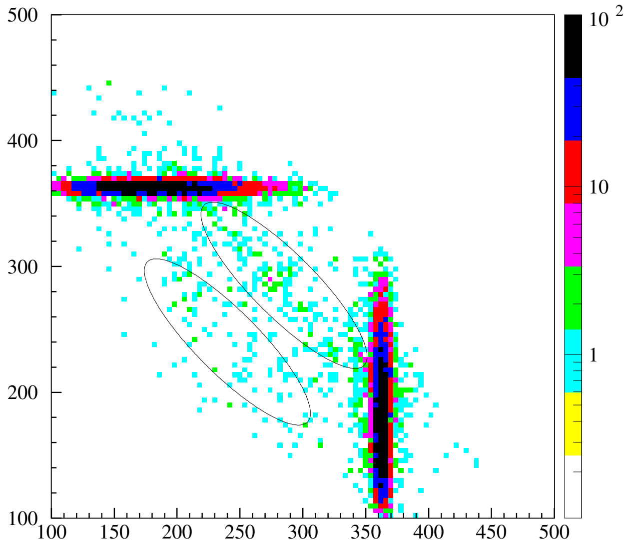


Figure 13: The $E_1$-$E_2$ plane on data.

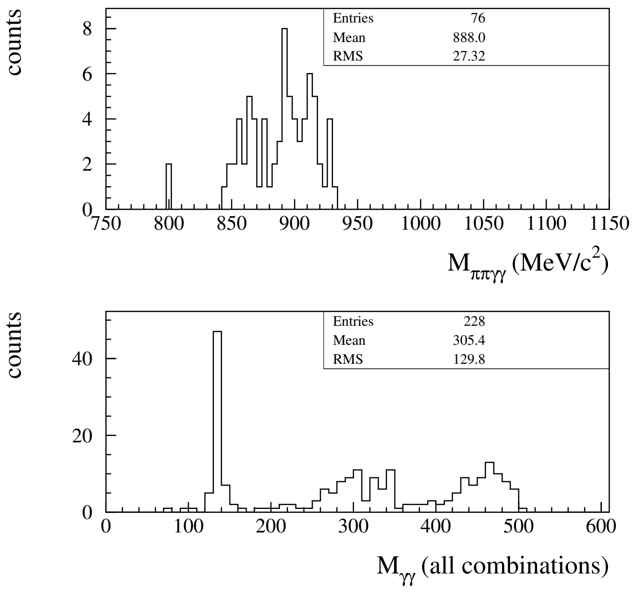


Figure 14: Distribution of $M_{\pi\pi\gamma\gamma}$ and of all combinations of $M_{\gamma\gamma}$ for events in the shifted "control" ellipse.

In order to count the background below our peak we have used two different methods, in which no input from Monte Carlo has been used, apart from the shape of the $\eta'$ mass peak.

- Method 1 : a fit on the $M_{\pi^+\pi^-\gamma\gamma}$ shape on data with a Gaussian + linear parameterization where mass and width of the Gaussian are fixed at the values obtained by Monte Carlo for pure $\phi \to \eta'\gamma$ events. With this method one has $N_{bkg} = 18 \pm 3$
- Method 2 : in order to better understand the shape of background on data a sidebands ellipse in the $E_1 - E_2$ plane, i.e. a "donuts shaped" region around the selection ellipse has been used, and the normalization for the $M_{\pi^+\pi^-\gamma\gamma}$ histogram has been fitted (shaded area), together with the normalization of the signal taken from Monte Carlo. We have used a binned likelihood fit in which also the finite statistics of signal and background histograms has been taken into account. With this method one has $N_{bkg} = 18 \pm 5$.

Finally we have to notice that a simple Monte Carlo evaluation of background, in which only $\phi \to \eta\gamma$ events survive, and using the ACCELE simulation for accidental clusters, gave a slightly lower value $N^{MC}_{bkg} = 12 \pm 3$. We compute the background evaluated with the "data driven" method and we decide, in order to be conservative, to use the higher error among the two: we thus estimate $N_{bkg} = 18 \pm 5$.

Since the number of event in the selected peak is 138 the final number of selected $\phi \to \eta'\gamma$ events is then evaluated as $N_{\eta'\gamma} = 120 \pm 12(\text{stat.}) \pm 5(\text{syst.})$. Monte Carlo efficiency for this selection on $\phi \to \eta'\gamma$ events is $\varepsilon_{\eta'\gamma} = 22.8\%$

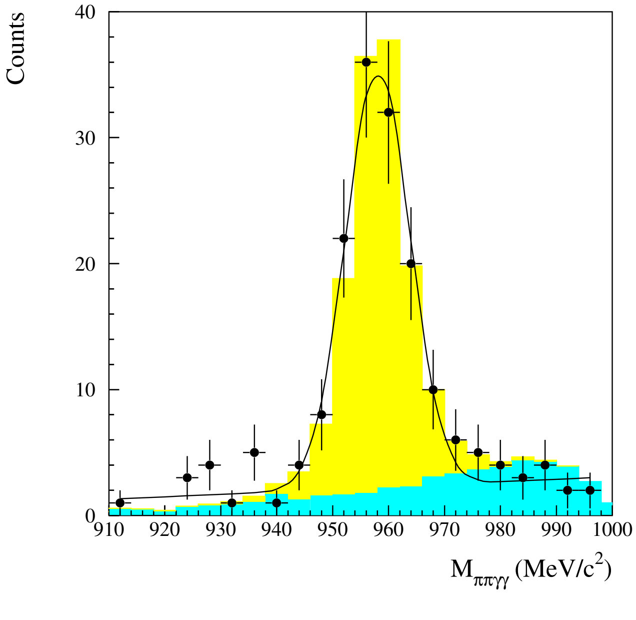


Figure 15: The $\pi^+\pi^-\gamma\gamma$ invariant mass for events selected as $\phi \to \eta'\gamma$ candidates. The shaded area is the sum of background obtained selecting events around the elliptical region and of the Monte Carlo shape of the signal, normalized to the result of the binned likelihood fit. The continuous line is the result of a Gaussian plus linear fit.

The angular distribution of the radiative photon for the selected $\phi \to \eta\gamma$ and $\phi \to \eta'\gamma$ events is compared to the Monte Carlo expected distribution, which for magnetic dipole transitions is expected to be $\propto (1 + \cos^2\theta)$. Results are shown in fig.16: we notice that the $\phi \to \eta\gamma$ distribution is flattened w.r.t. the original $(1 + \cos^2\theta)$ shape due to the tracking inefficiency for high $\cot\theta$ and the correlation between the $\cot\theta$ of the tracks and the radiative photon angle. This effect is not present in $\phi \to \eta'\gamma$ events where the radiative photon is the softest one. The distribution found for $\phi \to \eta'\gamma$ events, though clearly not yet statistically relevant, does not contradict the expected Monte Carlo shape.

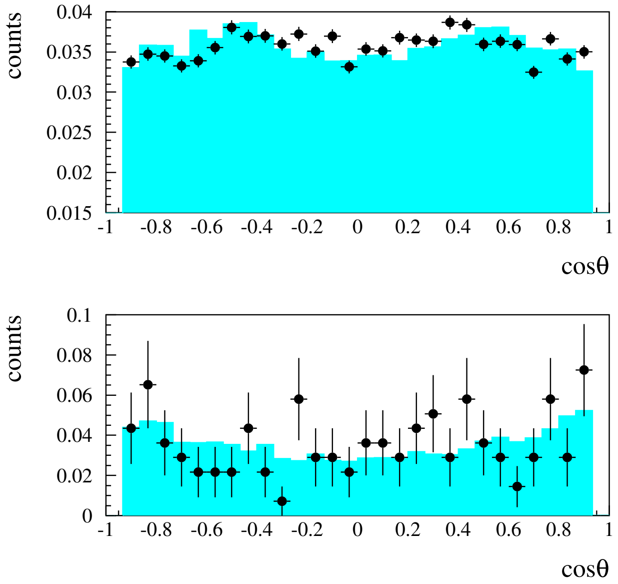


Figure 16: Angular distributions of the radiative photon: data (dots) versus Monte Carlo (histo) for $\phi \to \eta\gamma$ events (upper plot) and $\phi \to \eta'\gamma$ events (lower plot).

## 4.4 Systematic checks

As a general strategy two kinds of systematics checks have been performed:

- control the distributions on which the cuts are set using the $\phi \to \eta\gamma$ sample;
- evaluate the shift on the ratio of counts, normalized to efficiencies: $R_N = \frac{N_{\eta'\gamma}}{N_{\eta\gamma}} \cdot \frac{\varepsilon_{\eta\gamma}}{\varepsilon_{\eta'\gamma}}$ after a change in some part of the analysis. The value has been compared to the central value of $R_N = 3.83 \cdot 10^{-3}$ obtained with the "standard" analysis described above.

The photon energies and the pion momenta (the variables on which the second level cuts are set) have been already shown before (see fig. 7) for the comparison data Monte Carlo on the control sample. Agreement is very good, and thus the systematic effect introduced by these cuts will be neglected in what follows.

The uncertainty on the $\mathcal{P}\chi^2$ cut, depends on the tail of the $\chi^2$ distributions and is not trivial to evaluate. In order to estimate this effect we have performed the whole analysis with different $\mathcal{P}\chi^2$ cuts in a range between 1% and $10^{-12}$, evaluating each time the ratio $R_N$ the maximum variation observed on $R_N$ has been of 2.3%.

| Effect | $\Delta R_N/R_N$ (max) |
|---|---|
| $\mathcal{P}(\chi^2)$ cut | 2.3% |
| Vtx eff. | 0.9% |
| Accidental rate | 0.5% |
| EVCL | 2.2% |

Table 4: Maximum observed variations on $R_N$.

To check the dependency on the charged vertex efficiency we have selected only the $\phi \to \eta\gamma$ events in the kinematical region allowed for the $\phi \to \eta'\gamma$ pions. This results in a ratio of efficiencies between $\phi \to \eta\gamma$ and $\phi \to \eta'\gamma$ events close to one (0.95). The value obtained in this way is $R_N = 3.86 \cdot 10^{-3}$.

In order to check the dependence of the analysis on the accidental rate we have raised the angular cut and the lower photon energy cut to 23° and 20 MeV respectively. These values were motivated by the observation of the distribution of accidental clusters which show a clear cutoff in this energy/angular region. The value of $R_N$, was found to be $3.81 \cdot 10^{-3}$.

In order to see if a bias was introduced by event classification the analysis has been repeated on a sample of events filtered only with very simple cuts described before (see sect. 3.4). When using the same statistics the discrepancy on $R_N$ with this method was found to be 2.2%.

All these results have been summarized in table 4.

As a further check the analysis has been repeated using two different approaches:

- Using the analysis technique adopted for 1999 data, in which a fully constrained kinematic fit was performed and the $\phi \to \eta'\gamma$ events selected with a simple cut on $\mathcal{P}(\chi^2)$ in the two hypotheses (see [13, 22] for details). About half of the statistics has been analyzed in this way. Result obtained is $R_N = (3.85 \pm 0.5(\text{stat.})) \cdot 10^{-3}$ .

- Fitting the $\gamma\gamma$ invariant mass peak of the two hardest photons ($M_{12}$) on a sample in which no ellipse cut was performed. In order to suppress background we veto a $4\sigma$ region around the $\pi^0$ mass for the invariant mass of the combination with the two *softest* photons in the event. $\phi \to \eta'\gamma$ events should show a clear peak at the value of the $\eta$ mass, as indeed is observed (see fig. 17). In this way we obtain $R_N = (3.94 \pm 0.45(\text{stat.}) \pm 0.39(\text{bkg})) \cdot 10^{-3}$ where the second error takes into account the dependence on the background absolute level and shape, obtained fitting the background with different parameterizations and sidebands.

We have also checked the stability of $\phi \to \eta'\gamma$ selection along data taking, though the low statistics does not allow a very significant scan. We show the result for the number of selected $\phi \to \eta'\gamma$ events over the $\phi \to \eta\gamma$ in intervals of about $3\,\text{pb}^{-1}$(see fig. 18). This number is somewhat larger than the one quoted in tab 5 ($2.7 \cdot 10^{-3}$ instead of $2.39 \cdot 10^{-3}$) since we here just count the events in the peak without attempting any background subtraction on the $3\,\text{pb}^{-1}$samples.

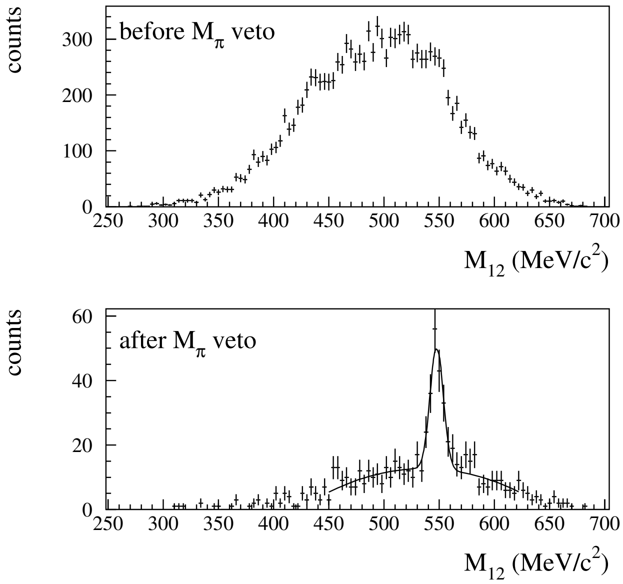


Figure 17: The invariant mass of the two hardest photons in $\pi\pi\gamma\gamma\gamma$ events. Upper plot: events passing the common selection; Lower plot: after a $4\sigma$ veto around the $\pi^0$ mass for the invariant mass of the two softest photons.

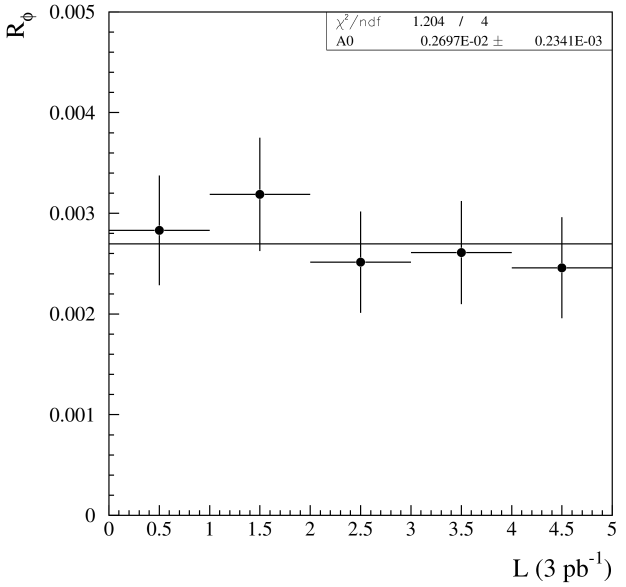


Figure 18: Selected number of $\phi \to \eta'\gamma$ / $\phi \to \eta\gamma$ events. Each point corresponds to $3\,\mathrm{pb}^{-1}$ of integrated luminosity.

# 5 Results

The ratio on the number of events selected as $\eta'\gamma$ and $\eta\gamma$ respectively, can be related to the ratio of the branching fractions $R = BR(\phi \to \eta'\gamma)/BR(\phi \to \eta\gamma)$ as follows:

$$R = \frac{N_{\eta'\gamma}}{N_{\eta\gamma}} \left(\frac{\varepsilon_{\eta\gamma}}{\varepsilon_{\eta'\gamma}}\right) \times \frac{BR(\eta \to \pi^+\pi^-\pi^0)BR(\pi^0 \to \gamma\gamma)}{BR(\eta' \to \pi^+\pi^-\eta)BR(\eta \to \gamma\gamma)} \cdot K_\rho$$

The factor $K_\rho$ accounts for interference between the amplitudes $A(\phi \to \eta(\eta')\gamma)$ and $A(\rho \to \eta(\eta')\gamma)$ and has been evaluated as follows. The cross section of the process $e^+e^- \to P\gamma$ can be written in the Born approximation as:

$$\sigma(s) = 12\pi \left| \sum_V \frac{\Gamma_V e^{i\phi_V}}{D_\phi(s)} \sqrt{B_{VP}} \frac{m_V^3}{s^{3/2}} \frac{q^3(s)}{q_V^3} \right|^2$$

V stands for $\phi, \rho$ ($\omega$ contribution is negligible); $q(s)$ and $q_V$ represent the pseudoscalar meson momentum at center of mass energy $= \sqrt(s)$ and center of mass energy $= m_V$ respectively; $D_V(S)$ represents the propagator of the vector meson: for the $\phi$ we have used the simple Breit Wigner form $m_\phi^2 - s - i\Gamma_\phi\sqrt{s}$ while for the $\rho$ meson we have used the Gounaris Sakurai parameterization. $B_{VP}$ represents the product of branchng ratios of vector mesons into $e^+e^-$ and final state $f$, execpt in the case of $\rho \to \eta'\gamma$ where we have used:

$$B_{\rho\eta'} = BR(\rho \to e^+e^-)BR(\eta' \to \rho\gamma) \cdot \frac{\Gamma_{\eta'}}{3\Gamma_\rho}$$

using the well known relation $\Gamma(P \to V\gamma) = 3\Gamma(V \to P\gamma)$.

The phases are fixed by the quark model, which imply destructive interference for the $\eta\gamma$ final state amplitudes and constructive interference for the ones with $\eta'\gamma$ in the final state. Using our central value for BR($\phi\eta'\gamma$) (in an iterative way) and all other values from PDG, we get the correction between the observed ratio of cross section to the needed ratio R: $K_\rho = 0.95$

Thus, using for all quantities in the above formula the values of table 5, where we summarize also the contributions to the final systematic error:

$$R = (4.70 \pm 0.47(\text{stat.}) \pm 0.31(\text{syst.})) \cdot 10^{-3}$$

| Quantity | Value | Syst. err. |
|---|---|---|
| $N_{\eta'\gamma}/N_{\eta\gamma}$ | $2.39 \cdot 10^{-3}$ | 4.2% (background) |
| $\left(\frac{\varepsilon_{\eta\gamma}}{\varepsilon_{\eta'\gamma}}\right)$ | 1.60 | Splitting 0.8%<br>Vtx eff. 0.9%<br>$\mathcal{P}(\chi^2)$ 2.3%<br>Accidentals 0.5%<br>EVCL 2.2% |
| $\frac{BR(\eta\to\pi^+\pi^-\pi^0)BR(\pi^0\to\gamma\gamma)}{BR(\eta'\to\pi^+\pi^-\eta)BR(\eta\to\gamma\gamma)}$ | 1.30 | 3.8% |
| TOTAL | | 6.6% |

Table 5: Contributions to the systematic error on $R$. The systematics evaluation on the ratio of analysis efficiencies is described in the previous sections. The intermediate BR's and errors are taken from [12].

The value we obtain for $R$ can be related directly to the mixing angle in the flavor basis. In the approach by Bramon *et al.* [5] where SU(3) breaking is taken into account via a constituent quark mass ratio $\frac{m_s}{\bar{m}}$ one has:

$$R = \frac{BR(\phi \to \eta'\gamma)}{BR(\phi \to \eta\gamma)} = \cot^2 \varphi_P \left(1 - \frac{m_s}{\bar{m}} \frac{\tan\varphi_V}{\sin 2\varphi_P}\right)^2 \left(\frac{p_{\eta'}}{p_\eta}\right)^3 \tag{1}$$

In the approach by Feldmann [7] chiral anomaly predictions for $P \to \gamma\gamma$ are combined with vector dominance to extract the couplings $g_{\phi\eta\gamma}$ and $g_{\phi\eta'\gamma}$ which yields, apart from OZI rule violation terms:

$$R = \frac{BR(\phi \to \eta'\gamma)}{BR(\phi \to \eta\gamma)} = \left(\frac{\sin\varphi_P\,\sin\varphi_V}{6f_q} - \frac{\cos\varphi_P}{3f_s}\right)^2 / \left(\frac{\cos\varphi_P\,\sin\varphi_V}{6f_q} + \frac{\sin\varphi_P}{3f_s}\right)^2 \left(\frac{p_{\eta'}}{p_\eta}\right)^3 \tag{2}$$

In both cases we use the result in the cited papers for all parameters entering the ratio except the mixing angle, in order to estimate the effect of our measurement on the angle $\varphi_P$ . We get essentially the same result in extracting the mixing angle in both approaches, i. e.

$$\varphi_P = \left(41.8^{+1.9}_{-1.6}\right)^\circ$$

in the first approach, and

$$\varphi_P = (42.2 \pm 1.7)^\circ$$

in the second one. A reasonable estimate of the theoretical uncertainties is given both by the difference of the two methods and by the difference between various $\varphi_P$ extractions using $m_s/\bar{m}$ in the range 1.24 - 1.45 (which is found in literature) for the first approach, and $f_s$ and $f_q$ within their errors as quoted in [7]. We conclude that the theoretical uncertainty in the extraction of the mixing angle is of order 0.5°. As far as the experimental errors are concerned we notice that the method we have used to evaluate them is not a trivial propagation in formulas 1-2, which would lead to an error of about 1.1°. This is because of the nonlinearity of the dependence of $\varphi_P$ on the ratio $R$. We have thus preferred to use a Monte Carlo extraction of $R$ with a Gaussian distribution using the total error as sigma, and then evaluated the 68% confidence interval on $\varphi_P$ .

This mixing angle would result in a mixing angle in the octet-singlet basis $\vartheta_P = \left(-12.9^{+1.9}_{-1.6}\right)^\circ$. Moreover, using the value in [12] for the BR($\phi \to \eta\gamma$ ) we can extract the most precise determination of BR($\phi \to \eta'\gamma$ ) to date (see fig. 19):

$$BR(\phi \to \eta'\gamma\ ) = (6.10 \pm 0.61\ (\text{stat.}) \pm 0.43\ (\text{syst.})) \cdot 10^{-5}$$

# 6 The gluonium content of the $\eta'$

One of the most important predictions of QCD is that the gluons are expected to form bound states with one another. In general these gluonic bound states can be expected to mix with neutral (isoscalar) mesons formed of quark-antiquark pairs, unless forbidden by $C$ and $P$ conservation. Search for "glueballs" (i. e. pure gluonium bound states) as well as for states including a gluonium admixture has been one of the most interesting issues of meson spectroscopy during last decades. A possible gluonium content of

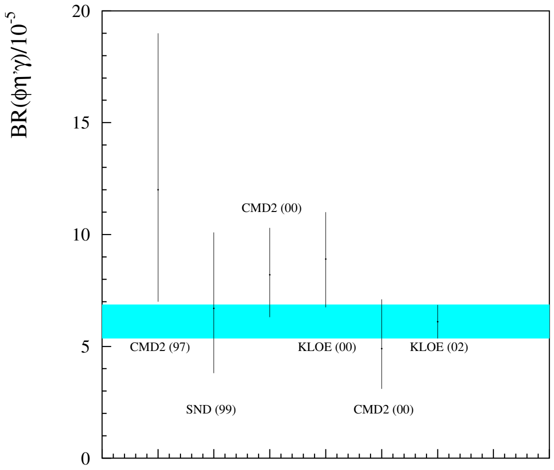


Figure 19: Determinations of the BR($\phi \to \eta'\gamma$ ) in literature: CMD2[25, 26, 27]; SND[24];KLOE(00)[13]; KLOE(02) : this work.

the $\eta'$meson has been argued for many years. An early study of a possible admixture of gluonium in the $\eta'$concluded [23] that a pure gluonium structure of the $\eta'$would lead to

$$\Gamma(\phi \to \eta'\gamma\ ) < 0.015 \;\; \text{keV} \tag{3}$$

that is $\mathcal{O}(10^{-6})$ for the BR($\phi \to \eta'\gamma$ ), and that a substantial gluonium component would be signalled by $\Gamma(\phi \to \eta'\gamma\ ) < 0.1$ keV that is BR($\phi \to \eta'\gamma$ )$< 2 \cdot 10^{-5}$. Further stress on the need of experimental data on the BR($\phi \to \eta'\gamma$ ) was pointed out by Rosner [3]. If we allow for gluonium admixture in $\eta'$(and/or in $\eta$ ) the mixing pattern of flavor states must be accordingly changed to

$$\begin{aligned} |\eta\rangle &= X_\eta \left|u\bar{u} + d\bar{d}\right\rangle/\sqrt{2} + Y_\eta \left|s\bar{s}\right\rangle + Z_\eta \left|glue\right\rangle \\ |\eta'\rangle &= X_{\eta'} \left|u\bar{u} + d\bar{d}\right\rangle/\sqrt{2} + Y_{\eta'} \left|s\bar{s}\right\rangle + Z_{\eta'} \left|glue\right\rangle \end{aligned} \tag{4}$$

with this notation in mind a possible gluonium content of the $\eta'$is revealed by:

$$Z^2_{\eta'} > 0 \Leftrightarrow X^2_{\eta'} + Y^2_{\eta'} < 1 \tag{5}$$

It is evident that in this case the mixing angle $\varphi_P$ cannot be extracted in the way we have done from the eqs. 1,2, where all OZI rule violating amplitudes have been neglected.
Constraints on $X_{\eta'}$ and $Y_{\eta'}$ can be obtained in a nearly model-independent way using simple SU(3) ideas, exploiting the magnetic dipole nature of the transitions VP$\gamma$ and PV$\gamma$ and evaluating ratios of BR's in order to normalize to one common coupling constant. The coupling to two photons is also quite understood theoretically and evaluated via the Wess-Zumino-Witten term of the chiral Lagrangian. Thus from

$$\frac{\Gamma(\eta' \to \rho\gamma)}{\Gamma(\omega \to \pi^0\gamma)} = 3\left(\frac{m^2_{\eta'} - m^2_\rho}{m^2_\omega - m^2_\pi}\frac{m_\omega}{m_{\eta'}}\right)^3 X^2_{\eta'} \tag{6}$$

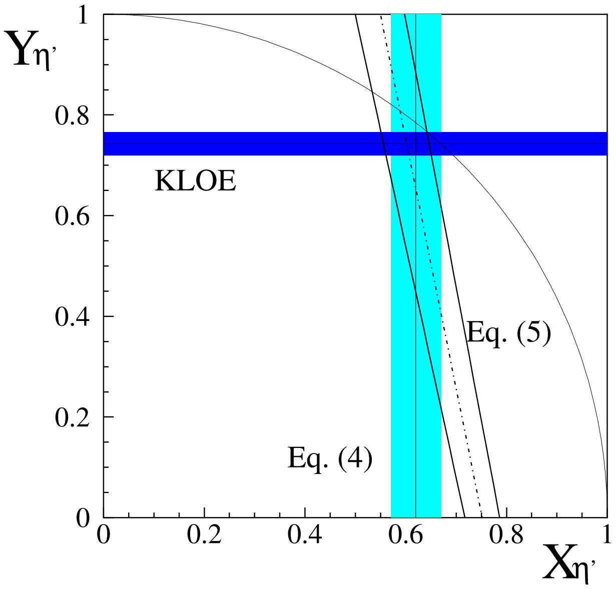


Figure 20: Bounds on $X_{\eta'}$ and $Y_{\eta'}$ from SU(3) calculations. In blue the KLOE result band in the assumption $Z_{\eta'} = 0$.

one gets constraints on $|X_{\eta'}|$ while from

$$\frac{\Gamma(\eta' \to \gamma\gamma)}{\Gamma(\pi^0 \to \gamma\gamma)} = \frac{1}{9}\left(\frac{m_{\eta'}}{m_{\pi^0}}\right)^3 (5X_{\eta'} + \sqrt{2}Y_{\eta'}\frac{f_q}{f_s})^2 \tag{7}$$

one gets constraints on $|X_{\eta'} + \frac{\sqrt{2}}{5}(\frac{f_q}{f_s})Y_{\eta'}|$. This is the approach followed for example in [3].

To check the gluonium content of the $\eta'$we control the self-consistency of our hypothesis: indeed if $Z_{\eta'} = 0$ then one has

$$|Y_{\eta'}| = \cos\varphi_P \tag{8}$$

This is also a reasonable approximation if the mixing with gluonium is not too large i. e. (as previously assumed), OZI rule violations are higher order corrections. We can then check if the region in the plane $|X_{\eta'}| - |Y_{\eta'}|$ where all allowed values overlap is consistent with $X^2_{\eta'} + Y^2_{\eta'} = 1$.

As already noticed values significantly lower than 1 for $X^2_{\eta'} + Y^2_{\eta'}$ would not fit into a simple $q\bar{q}$ scheme signalling a departure of $\eta'$structure from the standard picture and a significant gluonium content. In figure 20 we show the limits induced by the previously mentioned decays together with the $\cos\varphi_P$ measurement performed by KLOE. We can extract $Z^2_{\eta'} = 1 - X^2_{\eta'} - Y^2_{\eta'}$ from the three quantities $X_{\eta'}$, $Y_{\eta'}$ and $X_{\eta'} + aY_{\eta'}$ (with $a = \frac{\sqrt{2}}{5}\frac{f_q}{f_s}$) in three correlated ways. Building with a dummy Monte Carlo the covariance matrix, one can evaluate a $\chi^2$ which, minimized, gives $Z^2$ while the $\chi^2 + 1$ bound gives the error. The result can be afterwards compared to what can be estimated by just considering the area where the three allowed regions overlap. We then get $Z^2_{\eta'} = 0.06^{+0.09}_{-0.06}$ which is consistent with zero, even if a gluonium content at level 10-15% cannot be excluded at the present level of accuracy.

## 7 Summary

We present an analysis of about 16 $\mathrm{pb}^{-1}$of integrated luminosity at the DAΦNE collider. We obtain the best determination of the BR for the relatively rare process $\phi \to \eta'\gamma$ . The ratio of this BR to the $\phi \to \eta\gamma$ one helps clarifying the longstanding $\eta$-$\eta'$mixing angle puzzle, and its absolute value is consistent with the hypothesis of a gluonium content for the $\eta'$ meson below 15%.

## Acknowledgments

Many people helped me in this work, which has been discussed in many KLOE meetings. First of all I would like to thank the whole $\phi$ decays group, and especially Ada Farilla, Simona Giovannella and Camilla Di Donato within this group. I thank the referees Giorgio Capon and Antonella Antonelli for carefully following the development of this final version of the work and for giving me many suggestions on possible systematic checks. Last, but certainly not least, I have to thank Rafel Escribano for his friendliness and for the clarifying discussions on the $\eta - \eta'$ mixing puzzle.

## References

[1] C. Becchi and G. Morpurgo Phys. Rev **140**, B687 (1965)

[2] F. E. Close "Pseudoscalar mesons at DAΦNE" in "The DAΦNE phyisics handbook" vol. II (ed. L. Maiani, G. Pancheri and N. Paver, Frascati 1992)

[3] J. L. Rosner Phys. Rev. **D27**, 1101 (1983)

[4] A. Bramon, R. Escribano and M. D. Scadron Phys. Lett. **B403**, 339 (1997)

[5] A. Bramon, R. Escribano and M. D. Scadron Eur. Phys J. **C7**, 271 (1999)

[6] A. Bramon, R. Escribano and M. D. Scadron Phys. Lett. **B503**, 271 (2001)

[7] T. Feldmann, Int. Jou. Mod. Phys. **A15**, 159 (2000)

[8] R. Kaiser and H. Leutwyler, hep-ph/9806336

[9] R. Escribano and J. M. Frere, Phys. Lett. **B459**, 288 (1999)

[10] Th. Feldmann, P. Kroll, and B. Stech, Phys. Rev. **D58**, (1998)

[11] F. De Fazio and M. R. Pennington, JHEP 0007:051 (2000)

[12] The Particle Data Group (D. Groom *et al.*) Eur. Phys. Jou. **C15** (2000)

[13] "KLOE first result on hadronic physics", contributed paper to ICHEP 2000 (Osaka), hep-ex/0006036

[14] KLOE Collaboration, "KLOE: a general purpose detector for DAΦNE", LNF-92/019 (IR) (1992); KLOE Collaboration, "The KLOE detector - Technical Proposal", LNF-93/002 (IR) (1993).

[15] S. Guiducci et al., Proceedings of PAC99, New York, March 1999.

[16] F. Ambrosino *et al.* KLOE memo 225, 2000

[17] M. Incagli, private communication.

[18] A. Aloisio *et al.*, [KLOE Collaboration], hep-ex/0107022

[19] M. Adinolfi *et al.*, [KLOE Collaboration] Nucl. Instrum. Meth. **A461**, 344 (2001)

[20] S. Miscetti, private communication

[21] C. Di Donato, Ph.D. thesis, Università di Napoli (2001)

[22] F. Ambrosino, Ph.D. Thesis, Università di Napoli (1999)

[23] N. Deshpande and G. Eilam Phys. Rev. **D25**,270 (1980)

[24] M. N. Achasov *et al.* [SND Collaboration], JETP Lett. **69**, 97 (1999)

[25] R. R. Akhmetshin *et al.* [CMD-2 Collaboration], Phys. Lett. **B415**, 445 (1997).

[26] R. R. Akhmetshin *et al.* [CMD-2 Collaboration], Phys. Lett. **B473**, 337 (2000)

[27] R. R. Akhmetshin *et al.* [CMD-2 Collaboration], Phys. Lett. **B494**, 26 (2000)